Catalysis Science & Technology

PAPER

View Article Online
View Journal | View Issue

Cite this: *Catal. Sci. Technol.*, 2014, 4, 3917

Synthesis and functionalization of SSZ-13 as an NH_3-SCR catalyst

Alexander Shishkin,†* Hannes Kannisto, Per-Anders Carlsson, Hanna Härelind and Magnus Skoglundh

Received 27th March 2014,
Accepted 30th June 2014

DOI: 10.1039/c4cy00384e

www.rsc.org/catalysis

Hydrothermal synthesis of Na-SSZ-13 using a low concentration of the structure-directing agent *N*,*N*,*N*-trimethyl-1-adamantanimonium hydroxide and functionalization of the SSZ-13 framework through the introduction of Cu and Fe *via* ion exchange have been carried out. The prepared samples were characterized by XRD, SEM, and UV-vis spectroscopy, N_2 sorption, XRF and NH_3-TPD. It was found that relatively large iron oxide particles and well-dispersed Cu^{2+} species are formed as a result of ion exchange with iron and copper, respectively. Furthermore, the catalytic activity for NH_3 oxidation, NO oxidation and selective catalytic reduction of NO_x with ammonia (NH_3-SCR) was investigated both in the absence and in the presence of water. The functionalization of the SSZ-13 structure enhances the catalytic activity for NH_3-SCR significantly. While the NH_3-SCR activity is negligible for the Na-SSZ-13 sample, the Cu-SSZ-13 sample is highly active especially at low temperatures, and the Fe-SSZ-13 sample shows the highest activity at elevated temperatures.

1. Introduction

Zeolites are truly indispensable in many catalytic processes like fluid catalytic cracking, hydrocracking, dewaxing, production of octane boosters, hydrodesulphurization, Fischer–Tropsch synthesis, methanol-to-olefin reaction, aromatic alkylation, nitration, halogenation, nucleophilic substitution and addition, and many others.[1] More recently, zeolites have also been introduced for catalytic emission control, *e.g.*, reducing the emission levels of nitrogen oxides (NO_x) from both stationary and mobile sources.[2–4] In particular, zeolites promoted with transition metals such as copper and iron[3,5] have been proven to be active for the selective catalytic reduction of NO_x by ammonia (NH_3-SCR), which is currently considered as one of the preferred technologies for NO_x removal from lean exhaust gases in automotive applications.[3,6,7]

Hitherto, synthesis of catalysts that combine high activity for NH_3-SCR at low temperatures with hydrothermal stability at high temperatures[3] remains a challenge. Recently, it was reported that using small-pore zeolites might meet these requirements;[8,9] thus, in particular, zeolites having the chabazite (CHA) structure have attracted much attention.[5] Specifically, copper-exchanged SSZ-13 has been reported to show superior performance in both mentioned aspects.[10–12]

Competence Centre for Catalysis, Chalmers University of Technology, Göteborg, Sweden. E-mail: shishkin@chalmers.se; Tel: +46 31 772 2938
† Postal address: Competence Centre for Catalysis, Chalmers University of Technology, Kemivägen 10, SE-412 96 Göteborg, Sweden.

Several methods, including conventional aqueous ion exchange, chemical vapor ion exchange, solid-state ion exchange and others, can be used to introduce metals into zeolite frameworks.[3] However, it can be hard to utilize the full ion-exchange capacity of the zeolite due to several factors. For zeolites with a high silica-to-alumina mole ratio, the ion exchange can be limited by the low alumina content of the zeolite framework as the number of ion positions that can be utilized is few. Furthermore, for the zeolites with narrow channels and/or for large and multivalent ions to be introduced, steric hindrance may limit the ion exchange. In this connection, most of the transition metal cations are strongly solvated[13] and thus surrounded with hydration shells that enhance the steric hindrance of the solvated cation, hindering its entry in the narrow channels of the zeolite framework. Especially for iron, it has been reported[14] that complete ion exchange is difficult due to limited diffusion of the hydrated cation into the zeolite pores, which instead results in an increased tendency of iron to form iron oxide particles with low SCR activity.[3]

The zeolite SSZ-13 was first synthesized by Zones using organic nitrogen-containing cations derived from 1-adamantamine, 3-quinuclidinol, or 2-*exo*-aminonorbornane, which acts as a structure-directing agent (SDA) during the zeolite synthesis.[15] The SDA based on an *N*,*N*,*N*-trimethyl-1-adamantanimonium cation-containing compound (most often, hydroxide or iodide) has been shown to be superior and prevails to be used in relatively high concentrations for the synthesis of SSZ-13.[8,9,16–18] This

SDA is however expensive; thus, to improve the synthesis economy and facilitate commercialization of this SSZ-13 zeolite, reducing the amount of SDA during the zeolite synthesis would be desirable.[19]

The aim of the present study is to synthesize SSZ-13 by using a low amount of SDA and to functionalize the SSZ-13 framework with copper and iron. Special attention is paid to how the zeolite synthesis and functionalization with iron and copper influence the structural properties as well as the catalytic activity for NH_3-SCR both in the absence and in the presence of water.

2. Experimental methods

2.1. Synthesis of zeolite SSZ-13

Zeolite SSZ-13 was synthesized based on the method reported by Zones.[16] However, two important changes in the synthesis route were made, *i.e.*, the use of a 25% lower amount of the structure-directing agent *N*,*N*,*N*-trimethyl-1-adamantanimonium hydroxide and increased synthesis time. 40 g of 1.0 M NaOH (Sigma-Aldrich), 55.6 g of 0.54 M *N*,*N*,*N*-trimethyl-1-adamantanimonium hydroxide (Sachem, Inc.) and 64.4 g of Milli-Q water were mixed in a Teflon cup of a 0.45 L Parr autoclave for 15 min. Subsequently, 1.0 g of $Al(OH)_3$ (May & Baker) was added to the solution, which was mixed for another 15 min. Then after addition of 12.0 g of SiO_2 (Aldrich) and mixing for 15 min, the resultant solution was kept at 140 °C for 33 days without agitation. The synthesis time was deliberately long to ensure the formation of SSZ-13. However, it should be noted that the possibility to further optimize the parameters of the synthesis has been investigated. So, it was found that it is possible to prepare SSZ-13 in 6 days using a 15% less amount of SDA than was used in the original method.[16] Moreover, we also were able to prepare SSZ-13 in 14 days using 25% less amount of SDA than the original method.[16] However, in the present study we aim to present only the results of one sample, namely, the one prepared in 33 days using 25% less amount of the SDA, although keeping in mind that the parameters of the synthesis, *i.e.* synthesis time and the amount of SDA to be added, can be optimized in future studies. After the set synthesis time was up, the resulting product was washed with Milli-Q water, vacuum-filtered and air-dried at room temperature for 12 h. The dried powder was finally calcined in air at 550 °C for 8 h using an initial temperature ramp rate of 2 °C min^{-1} starting from RT to produce the sodium form of the zeolite. The mass of the final product (fine white powder) was 7.5 g, which corresponds to 65% yield of Na-SSZ-13 based on TO_2.

2.2. Functionalisation of SSZ-13

In order to obtain the zeolite in the NH_4 form, the calcined powder was ion exchanged using a 0.1 M solution (2.0 g of Na-SSZ-13 L^{-1}) of NH_4NO_3 (Fisher Scientific). The slurry was heated at 80 °C for 8 h using an oil bath, after which the powder was filtered, washed with Milli-Q water and finally air-dried at room temperature for 12 h.

A 0.5 L solution of 0.025 M $Cu(NO_3)_2$ was prepared by adding 2.91 g of $Cu(NO_3)_2{\cdot}2.5H_2O$ (Sigma-Aldrich) to 0.5 L of Milli-Q water. The pH of the solution was adjusted to 3.5 by addition of nitric acid (Fisher Scientific) with subsequent addition of the NH_4 zeolite to the $Cu(NO_3)_2$ solution (1.0 g of NH_4-SSZ-13 L^{-1}). The slurry was heated at 80 °C using an oil bath and stirred for 1 h, after which the slurry was filtered and washed with Milli-Q water. The resulting product was dried at room temperature for 12 h and finally calcined at 550 °C for 3 h in air at a ramp rate of 2 °C min^{-1} starting from RT.

A sample of the zeolite in the iron form was prepared by ion exchange in 0.5 L of 0.025 M $FeSO_4$ solution (1.0 g of NH_4-SSZ-13 L^{-1}). The $FeSO_4$ solution was prepared by adding 3.02 g of $FeSO_4{\cdot}5H_2O$ (Sigma-Aldrich) to 0.5 L of Milli-Q water. The pH of the solution was then adjusted to 2.5 by addition of sulphuric acid (Merck). The slurry was stirred and heated at 90 °C for 2 h using an oil bath and subsequently vacuum-filtered and washed with 3 L of Milli-Q water. A higher temperature was used during the Fe-exchange process compared to the corresponding ion exchange with copper in order to compensate for the effect of the difference in the size of solvation shells, which are formed in water solutions of iron and copper salts,[20] and hence facilitate the penetration of iron into the zeolite channels. The resulting product was dried at room temperature for 12 h and finally calcined at 550 °C for 3 h in air at a ramp rate of 2 °C min^{-1} starting from RT.

2.3. Catalyst characterization

The physical and chemical properties of the prepared samples were characterized using several methods.

Quantitative analysis of the elemental composition of the samples was performed by X-ray fluorescence (XRF) using a PANalytical PW2424 instrument and the software UniQuant 5.0.

The specific surface area and the pore volume of the samples were determined by nitrogen sorption at −196 °C using a Micromeritics TriStar 3000 instrument.

The crystal phases of the samples were determined by X-ray diffraction (XRD) using a Siemens D5000 diffractometer scanning 2θ from 5 to 50° in the scan mode (0.02°, 1 s). Ni-filtered Cu Kα radiation (λ = 1.54187 Å) was used for the analysis.

The shape and morphology of the crystals of the as-prepared sample in the sodium form were studied by scanning electron microscopy (SEM) using an FEI Quanta 200 FEG environmental scanning electron microscope equipped with an Oxford INCA energy-dispersive X-ray (EDX) analysis system. An acceleration voltage of 20 kV, a working distance of 11.9–12.0 mm, and a spot size of 3 were used during the SEM analysis, which was performed in the secondary electron mode by using an Everhart–Thornley detector.

The acidity of the samples was characterized using temperature-programmed desorption (TPD) of NH_3. The TPD

experiments were performed by exposing the sample (63.3 mg of Na-SSZ-13, 78.7 mg of Fe-SSZ-13 and 92.8 mg of Cu-SSZ-13) to 400 ppm NH_3 at 150 °C until saturation followed by flushing with Ar for 30 min. The latter step was followed by a temperature ramp from 150 to 500 °C in Ar at a heating rate of 10 °C min^{-1}. The total gas flow was kept constant at 300 ml min^{-1}, which corresponds to a space velocity (GHSV) of 205 000 h^{-1}.

The nature of the iron and copper species in the exchanged samples was studied by diffuse reflectance UV-Vis spectroscopy. The spectra were collected using a Cary 5000 UV-Vis–NIR spectrophotometer equipped with an external DRA-2500 unit. The integrating sphere permits fast acquisition of high-quality (high-resolution, low-noise) spectra. The reflectance spectra were recorded in the 200–870 nm wavelength range using the appropriate baseline correction, and the spectrum of the Na-SSZ-13 zeolite was subtracted as part of the background.

2.4. Flow reactor experiments

The catalytic performance of the prepared samples was evaluated in a continuous gas flow reactor system consisting of a vertically placed quartz tube (L = 260 mm, d = 4 mm) equipped with an insulated metal coil for resistive heating. The catalytic bed temperature was measured by a type K thermocouple and controlled by a PID regulator (Eurotherm). A quartz bed (h = 70 mm) was placed before the catalytic bed and the catalytic bed (h = 7 mm) was placed on top of the quartz bed. The gas mixing system consists of separate mass flow controllers (Bronkhorst Low ΔP) for NO, NH_3, O_2 and Ar. Water was added separately to the reactor system *via* a controlled evaporator mixer system (CEM, Bronkhorst Hi-Tech). The inlet of the gas/water mixture to the reactor was placed 150 mm below the quartz bed. The composition of the gas phase was continuously analyzed by FTIR spectroscopy (MKS 2030 FTIR spectrometer).

Steady-state activity tests were performed for all samples (with the same sample amounts as in the NH_3-TPD experiments) using a gas composition of 400 ppm NO and/or 400 ppm NH_3, 0 or 6% H_2O and 8% O_2 in Ar. The total gas flow was kept constant at 300 ml min^{-1}, which corresponds to a space velocity (GHSV) of 205 000 h^{-1}. To investigate the activity for NO oxidation and NH_3 oxidation, the samples were exposed to 400 ppm NO or 400 ppm NH_3, respectively, and 8% O_2 in Ar whereby the sample temperature was increased stepwise from 150 to 500 °C (150, 200, 250, 300, 350, 400 and 500 °C). The temperature was kept constant for 45 min at each temperature step. The heating rate between the temperature steps was 20 °C min^{-1} and the temperature did not exceed the set point by more than 5 °C before stabilization at each step. The activity for selective catalytic reduction of NO_x with ammonia was studied for all samples, similar to the oxidation experiments. In the NH_3-SCR experiments, the gas feed consisted of 400 ppm NO, 400 ppm NH_3, 0 or 6% H_2O, and 8% O_2 in Ar.

3. Results and discussion

In this section, we describe and discuss the results of the synthesis and characterization of the functionalized SSZ-13 samples as well as the analysis of how these materials function as NH_3-SCR catalysts.

3.1. Structure, composition and acidity of the Me-SSZ-13 zeolites

The yield of Na-SSZ-13 based on TO_2 was 65%. This is just 9% lower than the product yield obtained by Zones,[16] notwithstanding the use of a 25% lower amount of SDA in the present study. This clearly shows that the synthesis of SSZ-13 can significantly be improved in order to achieve a higher relative yield of the zeolite (based on the ratio between the mass of the final product and the mass of the used SDA).

The resultant material from the zeolite synthesis was identified and confirmed as the SSZ-13 zeolite structure using X-ray diffraction. Fig. 1 shows the XRD patterns of the as-prepared Na-SSZ-13, Cu-SSZ-13 and Fe-SSZ-13 materials. Based on the XRD peaks, which for all samples are highly intensive, we can conclude that they represent highly crystalline materials. Furthermore, the XRD peaks match the characteristic peak positions of the SSZ-13 structure.[16] It can be noted though that the relative intensities of some peaks, *i.e.* at 2θ = 13.2, 14.2, 16.3, 18.1, 22.5, 22.8, 23.4°, differ from the characteristic SSZ-13 pattern. This can be explained by the different Si/Al ratios compared to that of the SSZ-13 sample in ref. 16. The Si/Al ratio is 13.3 and 8.4 for the reference and the prepared sample, respectively, resulting in diverse structure factors that influence the relative peak intensities.[21] No additional peaks, which can be attributed to other crystalline phases, such as iron oxides or copper oxides, were found. This indicates that no large (*i.e.* larger than 3–5 nm,[22]) iron or copper particles are present in the zeolite samples.

In order to visually conceive the shape and the size of the prepared zeolite crystals, the Na-SSZ-13 sample was analyzed by

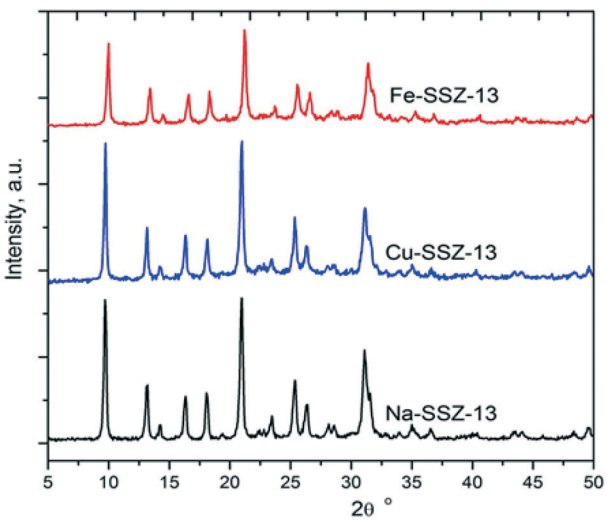

Fig. 1 X-ray diffractograms of the prepared Na-SSZ-13, Cu-SSZ-13 and Fe-SSZ-13 samples.

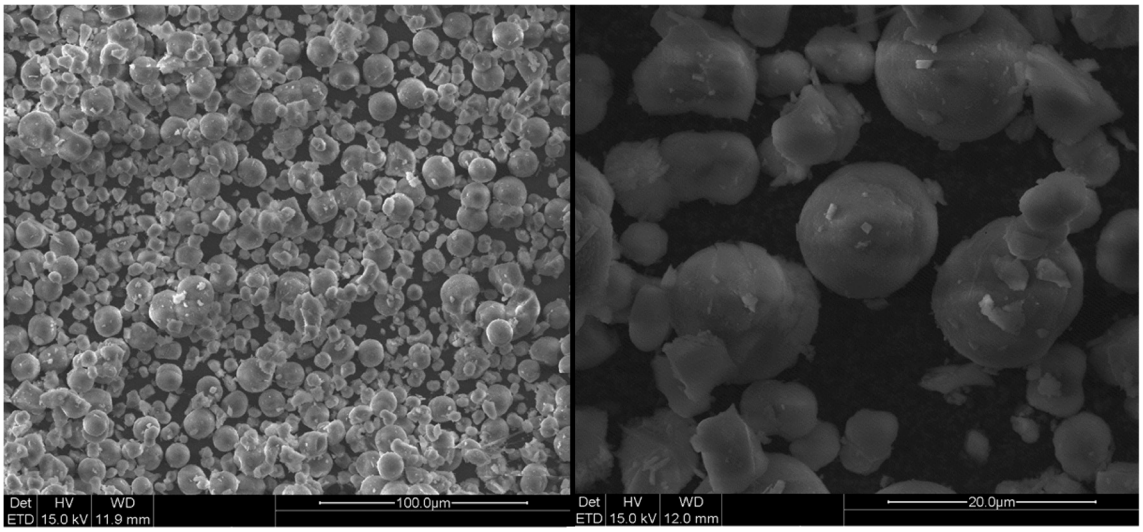

Fig. 2 Scanning electron microscopy images of the synthesized Na-SSZ-13 sample.

SEM. Generally, the morphology of zeolite SSZ-13 crystals depends on the preparation route.[9,17,23] In this work, the SEM images of the prepared SSZ-13 crystals (Fig. 2) show a predominant globe-shaped morphology with a particle size varying from 2 to 16 micrometers. Furthermore, a minor amount of outgrowths is present at the interface of the zeolite crystals. The outgrowths on the crystals were analyzed by EDX (not shown) and it was found that their elemental composition is nearly identical to that of the zeolite crystals. Hence, it can be concluded that the outgrowths most likely represent the same material, namely, Na-SSZ-13. The results of the EDX analysis are in good agreement with the results of the XRF analysis (Table 1).

In general, the NH_3-SCR activity of metal-exchanged zeolite catalysts correlates both with the type of metal and the degree of ion-exchange and with the framework type and the Si/Al ratio of the parent zeolite.[3] Hence, the chemical composition of the prepared samples, which is summarized in Table 1, is of vital importance. Although the molar concentrations of the iron and copper solutions were identical and a longer time for ion-exchange was used in the case of iron exchange, the resultant level of ion exchange was higher for copper. This can most likely be explained by the fact that iron is more difficult to introduce into the zeolite framework of SSZ-13 as compared to copper. This may arise from the different solvation abilities of the metal ions; hence, the formed Me^{n+}/water complex will differ in size. In this particular case, the Fe^{2+}/water solvation complexes are likely larger in comparison with the corresponding Cu^{2+}/water complexes.[20] Moreover, hydrated cations can be hydrolyzed and, under certain pH conditions, form stable intermediate products with higher positive charge, which can adsorb strongly to the negatively charged zeolite adsorption sites, according to the following reactions:[24]

$$\left[Me(H_2O)_y\right]^{n+}_{(aq)} \leftrightarrow \left[Me(OH)(H_2O)_{y-1}\right]^{(n-1)+}_{(aq)} + H^+_{(aq)} \leftrightarrow \left[(H_2O)_4Me\begin{matrix}OH\\ \diagup\ \diagdown\\ \diagdown\ \diagup\\ OH\end{matrix}Me(H_2O)_4\right]^{n+1}.$$

Table 1 Elemental composition of the prepared samples

	Amount (wt.%)		
Element	Na-SSZ-13	Cu-SSZ-13	Fe-SSZ-13
Na	2	<0.1	<0.1
Al	4	4	4
Cu	<0.02	3	<0.02
Fe	<0.02	<0.02	1
Si	40	40	40

The charge of such Fe and Cu complexes might also differ and hence affect the ion-exchange process.

UV-vis spectroscopy can be used to study the distribution of metal species in the metal-exchanged zeolites. We have previously studied the distribution of iron species in the iron-exchanged zeolite beta, Fe-BEA, using UV-vis spectroscopy.[25] Absorption in the 220–290 nm range represents monomeric iron species, dimeric and oligomeric iron species absorb at 300–400 nm and absorption above 400 nm is attributed to larger iron oxide particles.[26–28] Previously, monomeric and dimeric iron species have been shown to provide the active sites for NH_3-SCR in Fe-ZSM-5, while large iron particles are inactive for NH_3-SCR.[29] In Fig. 3a, the UV-vis spectrum of the Fe-SSZ-13 sample is shown. It can be clearly seen that for this sample all of the above-listed iron species are present, although iron oxide particles seem to be dominating. Comparing the present UV-vis study of the Fe-SSZ-13 sample with the study of Fe-BEA,[25] the fraction of monomeric, dimeric and oligomeric iron species is significantly lower for Fe-SSZ-13, while the fraction of iron particles is considerably lower for Fe-BEA. This is probably due to the smaller pore size of SSZ-13 compared to that of the zeolite BEA, which means that some of the iron species formed during the ion-exchange process likely cannot enter the pores. As a result, iron species agglomerate and larger iron particles are formed, most likely outside the microporous structure of SSZ-13. Such

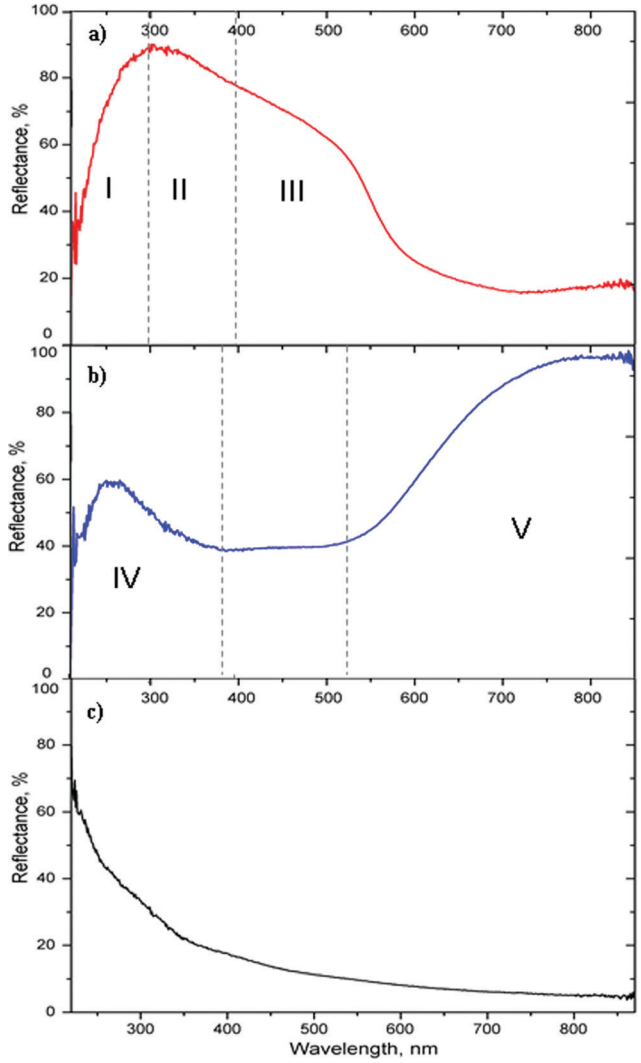

Fig. 3 UV-Vis spectra from the Fe-SSZ-13 (a) and Cu-SSZ-13 (b) powder samples after subtraction of the corresponding spectrum for the Na-SSZ-13 (c). Monomeric iron species are located in the region 220–300 nm (I), dimeric and oligomeric iron species are located in the region 300–400 nm (II), and larger iron oxide particles are located in the region >400 nm (III). Cu(I) and Cu(II) species in the zeolite framework are located in the region 220–380 nm (IV), Cu^{2+} ions in octahedral environment are located in the region >530 nm (V).

iron particles are sufficiently small not to be detected by XRD (see Fig. 1).

The UV-vis spectrum of the Cu-SSZ-13 sample is shown in Fig. 3b. There are two visible absorption bands. The first band, at wavelengths around 270 nm, is assigned to oxygen-to-metal charge transfer related to Cu(I) or Cu(II) species stabilized in the zeolite framework.[30–32] The origin of the broad band at wavelengths above 550 nm has been interpreted differently in the open literature.[32–35] On the one hand, Bennici *et al.*[33] suggested that the position of the absorption maximum of this band is dependent on the nuclearity of CuO_x clusters, *i.e.* the lower the wavelength of the absorption, the larger the clusters and *vice versa*. For example, for CuO_x/SiO_2–Al_2O_3 catalysts, Bennici *et al.*[33] reported a maximum of that band at 818 nm for a catalyst containing 0.23 wt.% CuO_x, whereas the corresponding maximum for a catalyst containing 12.4 wt.% CuO_x was observed at 754 nm. On the other hand, the same band at wavelengths above 550 nm was ascribed to Cu^{2+} ions in an octahedral environment where the exact position depends on the hydration degree, in other words, on the number of H_2O ligands bound to Cu^{2+}.[34,35] In our study, the absorption maximum of this band is observed around 820 nm. Despite the relatively high copper loading, 3 wt.% in our SSZ-13 sample, the position of the maximum of this band is close to that obtained for the CuO_x/SiO_2–Al_2O_3 sample with low copper loading in ref. 33, possibly indicating small and well-dispersed CuO_x clusters. It is, however, even more likely that our UV-vis data reflect the presence of Cu^{2+} ions. This explains the fact that the Cu-SSZ-13 sample is highly active for NH_3-SCR (see below), in line with previous studies.[18,36]

The catalytic properties of zeolites are often determined by the microporous structure of the zeolite.[37,38] The microporosity of the synthesized zeolite samples in the present work was studied using N_2 physisorption. The measured BET surface areas of the prepared samples are listed in Table 2. It should be noted though that for N_2 adsorption, the BET method has fundamental limitations when applied to zeolites, particularly for small-pore zeolites such as CHA. This is due to the fact that some assumptions behind the BET analysis are strictly not applicable in the presence of micropores,[39] which may lead to negative C values[17] in the BET equation. However, although the surface area obtained by applying the BET method for adsorption isotherms of microporous solids does not reflect the true internal surface area, it can be used for empirical comparisons.[40] In this study, the BET surface area and the pore volume of the Na-SSZ-13 sample are 611 $m^2\ g^{-1}$ and 0.29 ml g^{-1}, respectively, which are in good agreement with other reports.[23,41,42] After ion exchange, the specific surface area and the pore volume of both metal ion-exchanged samples decrease by about 27 and 23%, respectively, compared to those of the parent Na-SSZ-13 zeolite. Such decrease in the surface area after ion exchange is significantly more pronounced for the small-pore-sized SSZ-13 zeolite than for medium- and large-pore-sized zeolites, such as ZSM-5, ZSM-11, and BEA.[43–45] Therefore, we conclude that the pore size is an important factor that strongly affects the obtained surface area of ion-exchanged zeolites.

It is well known that acidic sites play an important role for NH_3-SCR. Therefore, NH_3-TPD experiments were performed in order to characterize the acidic properties of the catalysts. The

Table 2 Specific surface area and pore volume of the prepared samples

Sample	BET surface area ($m^2\ g^{-1}$)	Pore volume (ml g^{-1})
Na-SSZ-13	611	0.292
Cu-SSZ-13	448	0.226
Fe-SSZ-13	438	0.222

strength of the acidic sites can be qualitatively estimated by the desorption temperature for ammonia where a high desorption temperature indicates strongly bound ammonia and hence strong acidic sites and *vice versa*. The stronger the acidic sites, the stronger the ammonia is bound, hence, the higher temperature required for ammonia desorption. The NH_3-TPD profiles of the prepared samples are shown in Fig. 4. All samples exhibit ammonia desorption both at low and intermediate/high temperatures, which correspond to loosely bound ammonia and chemisorbed ammonia on Lewis and/or Brønsted acid sites.

The shape of the ammonia desorption profiles differs for the three samples. The ammonia desorption of the Na-SSZ-13 and Fe-SSZ-13 samples is essentially completed before reaching 500 °C, contrary to what is observed for the Cu-SSZ-13 sample where NH_3 desorption is still significant at 500 °C.

For the copper-exchanged sample, the NH_3-TPD profile represents a complex curve, which can in principle be deconvoluted by any number of curves. However, three main pronounced peaks at 220, 380, and 450 °C can be more easily distinguished and marked out among the others. Each of these peaks corresponds to certain sites where ammonia is bound, both at the medium-temperature region and, predominantly, at the high-temperature region. On the contrary, for the Na-SSZ-13 and Fe-SSZ-13 samples fewer intersecting adsorption peaks appear, and their maxima appear in the medium temperature range (250 and 300 °C, respectively). All peak positions are in agreement with previously reported results for different Na-, Cu- and Fe-zeolites.[44,46–48] It can also be observed that for the Na-SSZ-13 and Fe-SSZ-13 samples, the amount of desorbed ammonia at lower temperatures is in general higher than at higher temperatures.

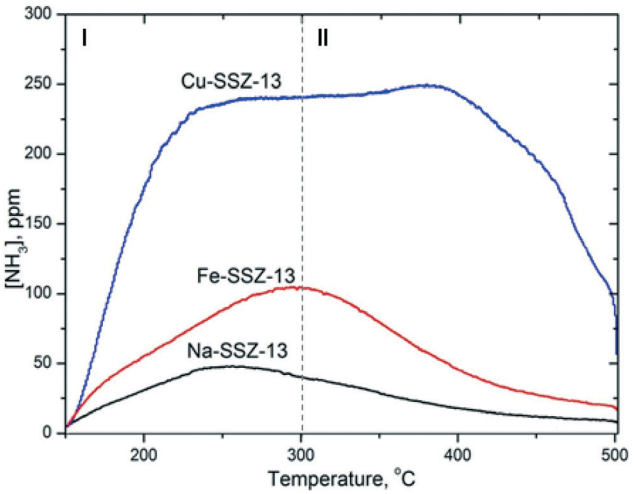

Fig. 4 NH_3 desorption profiles for the Na-SSZ-13 (63.3 mg), Cu-SSZ-13 (92.8 mg), Fe-SSZ-13 (78.7 mg) samples. All samples were exposed to 400 ppm NH_3 for 2 h at 150 °C, followed by flushing with Ar for 30 min. This was finally followed by a temperature ramp (heating rate 10 °C min^{-1}) from 150 to 500 °C in Ar. GHSV = 205 000 h^{-1}. Area I represents the medium-temperature region. Area II represents the high-temperature region.

The ammonia adsorption capacity of the samples is shown in the Table 3. The amount of ammonia released from the Cu-SSZ-13 sample during the TPD is 1.50 mmol g_{sample}^{-1}, while the corresponding amounts released from the Fe-SSZ-13 and Na-SSZ-13 samples are only 0.52 and 0.30 mmol g_{sample}^{-1}, respectively. The ability of the Cu-exchanged SSZ-13 sample to store a higher amount of ammonia as compared to the Na-SSZ-13 and Fe-SSZ-13 samples is likely due to the fact that the number of adsorbed ammonia molecules per metal site is higher for copper than for sodium and iron. This is in good agreement with the previously reported results. For example, Komatsu *et al.*[49] proposed that up to four ammonia molecules can be coordinated to each copper site at room temperature, whereas in the case of iron, only up to two ammonia molecules can be coordinated to each site.[46] However, the temperature also affects the number of NH_3 molecules adsorbed during the NH_3-TPD experiment. If the adsorption takes place at elevated temperatures, one should expect a lower number than four and two ammonia molecules adsorbed per copper and iron site, respectively. Another reason for the higher NH_3-storage capacity of Cu-SSZ-13 is likely due to the higher dispersion of copper in this sample compared to the dispersion of iron in the Fe-SSZ-13 sample. Hence, there are more available adsorption sites for NH_3 in the Cu-SSZ-13 sample than in the Fe-SSZ-13 sample.

3.2. Catalytic activity for NH_3-SCR

In Fig. 5, the catalytic activity for NH_3-SCR over the Na-SSZ-13, Cu-SSZ-13 and Fe-SSZ-13 samples is shown. The top panel shows the NO_x conversion and the bottom panel shows the corresponding conversion of ammonia, both in the absence and in the presence of 6% water.

In the absence of water, the Na-SSZ-13 sample exhibits minor NO_x reduction. In the temperature range studied, the highest conversion is only 5% at 500 °C. However, for the iron- and copper-exchanged SSZ-13 samples, the NO_x reduction is much higher. For the Cu-SSZ-13 sample, the NO_x reduction is particularly high at low temperatures, resulting in an almost complete NO_x conversion (98%) between 250 and 300 °C. The Fe-SSZ-13 sample shows relatively low NO_x reduction at low temperatures (below 300 °C) but at higher temperatures the NO_x reduction increases considerably, reaching 62% at 500 °C.

The presence of water clearly influences the catalytic behavior. The minor NO_x reduction observed for the Na-SSZ-13 sample in the absence of water is suppressed to negligible levels when water is present in the feed. In this case, the

Table 3 Amount of NH_3 desorbed during the NH_3-TPD experiments

Sample	NH_3 uptake (mmol g_{sample}^{-1})
Na-SSZ-13	0.30
Cu-SSZ-13	1.50
Fe-SSZ-13	0.52

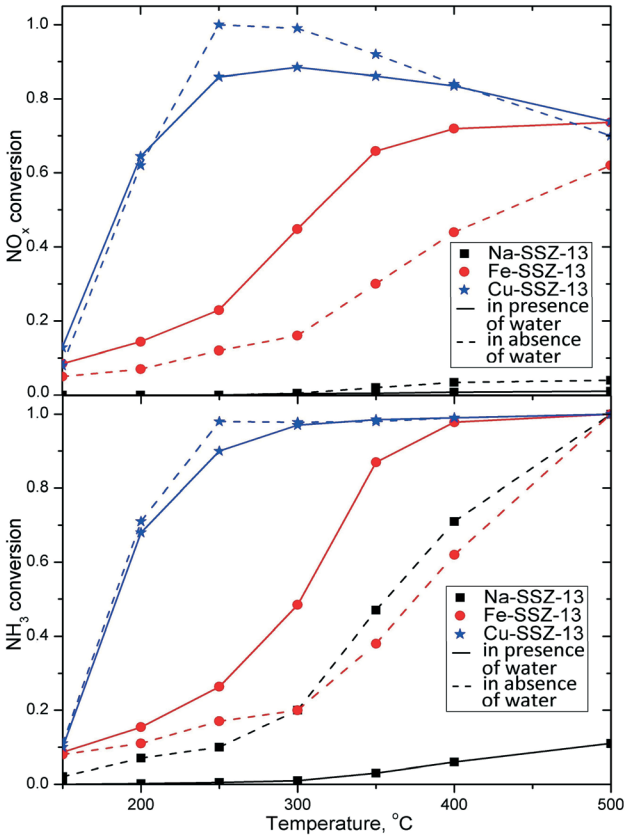

Fig. 5 NH_3 and NO_x conversion during NH_3-SCR in the presence (solid lines) and in the absence (dashed lines) of water for the following samples: 63.3 mg of Na-SSZ-13 (black lines with squares), 78.7 mg of Fe-SSZ-13 (red lines with circles) and 92.8 mg of Cu-SSZ-13 (blue lines with stars). All samples were exposed to 400 ppm NH_3, 400 ppm NO, 0 or 5% H_2O and 8% O_2 in Ar (balance) at 150, 200, 250, 300, 400 and 500 °C for 45 min for each step. GHSV = 205 000 h^{-1}.

conversion is below 1%. In the case of the Cu-SSZ-13 sample, water suppresses the activity at low temperatures with a maximum of 88% at 300 °C; however at temperatures above 400 °C, the activity for NO_x reduction in the presence of water is somewhat higher than in the absence of water. In contrast, the Fe-SSZ-13 sample is generally more active for NO_x reduction in the presence than in the absence of water. As a result, the NO_x conversion of the Fe-SSZ-13 sample reaches 75% at 500 °C. Hence, the presence of water has a strong positive effect on the NH_3-SCR activity over the iron-exchanged sample. It has been suggested that water participates in the SCR reaction (see *e.g.* the review by Brandenberger *et al.*[3]). Our data suggest that water participates differently in the SCR reaction over the Cu-SSZ-13 (and Na-SSZ-13) and Fe-SSZ-13 samples. This may be related to the fact that we have different types and distributions of the active species (metal and cluster size). However, to reveal the true reaction mechanism is not straightforward and is beyond the scope of the present study. It should also be noticed that for all samples, a so-called overconsumption of NH_3 (ref. 50) was observed especially at high temperatures (above 300 °C). This can be explained by NH_3 oxidation with oxygen, which particularly occurs under these reaction conditions.

The catalytic performance of the Na-SSZ-13, Cu-SSZ-13 and Fe-SSZ-13 samples for NO and NH_3 oxidation is shown in Fig. 6 and 7, respectively.

In addition, in Fig. 6 the equilibrium conversion of NO, *i.e.* the highest conversion of NO that can be achieved considering the thermodynamics, is shown. For all catalysts, the NO

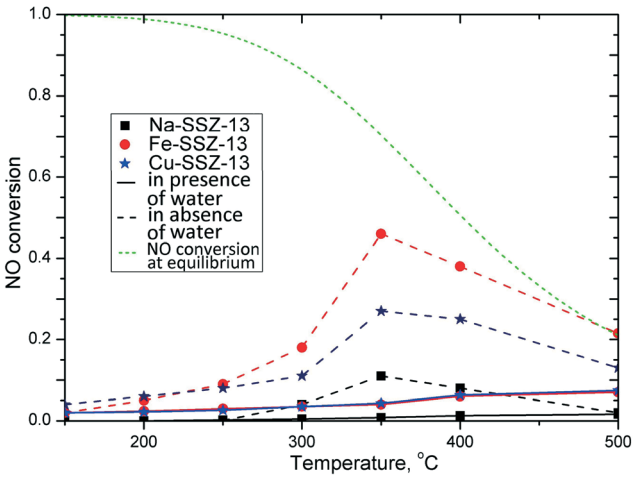

Fig. 6 NO conversion during NO oxidation in the presence (solid lines) and in the absence (dashed lines) of water for the following samples: 63.3 mg of Na-SSZ-13 (black lines with squares), 78.7 mg of Fe-SSZ-13 (red lines with circles) and 92.8 mg of Cu-SSZ-13 (blue lines with stars). All samples were exposed to 400 ppm NO, 0 or 5% H_2O and 8% O_2 in Ar (balance) at 150, 200, 250, 300, 400 and 500 °C for 45 min for each step. GHSV = 205 000 h^{-1}. The equilibrium conversion of NO is shown by the green dashed line.

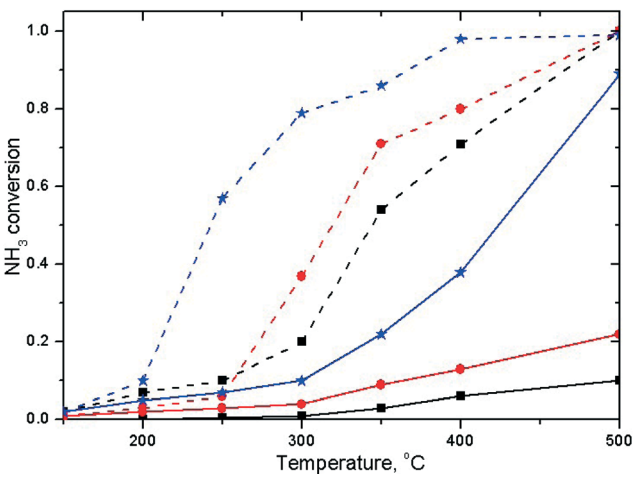

Fig. 7 NH_3 conversion during NH_3 oxidation in the presence (solid lines) and in the absence (dashed lines) of water for the following samples: 63.3 mg of Na-SSZ-13 (black lines with squares), 78.7 mg of Fe-SSZ-13 (red lines with circles) and 92.8 mg of Cu-SSZ-13 (blue lines with stars). All samples were exposed to 400 ppm NH_3, 0 or 5% H_2O and 8% O_2 in Ar (balance) at 150, 200, 250, 300, 400 and 500 °C for 45 min for each step. GHSV = 205 000 h^{-1}.

conversion is kinetically limited below 350 °C. The observed maximum in NO conversion in the absence of water is more difficult to explain. For all catalysts and also in other studies (see *e.g.* ref. 51–53), it occurs around 350 °C, which is also in the temperature region where the calculated equilibrium composition between NO and NO_2 is 1 : 1.

The Fe-SSZ-13 sample is the most active sample for NO oxidation and the NO oxidation for this sample reaches 58% at 350 °C. The Cu-SSZ-13 sample exhibits lower activity for NO oxidation with an observed highest conversion of 27% at 350 °C. Over the Na-SSZ-13 sample, the NO oxidation reaches only 12% at the highest. Despite the fact that the conversion of NO is relatively high in the absence of water, the catalytic activity for NO oxidation is much lower in the presence of 6% water. However for all samples, the NO oxidation increases slightly with increasing temperature. The lower NO oxidation in the presence of water can be explained by inhibition of active sites by water; therefore, only low conversion of NO to NO_2 is achieved in the presence of water.[43]

The catalytic performance for NH_3 oxidation is found to be considerably higher in the absence than in the presence of water for all samples. During the NH_3 oxidation experiments, the formation of NO, NO_2 and N_2O never exceeded a few ppm, and therefore, these figures are not reported. The most active catalyst is the Cu-SSZ-13 sample, both in the absence and in the presence of water. The difference in catalytic activity is strongly pronounced especially in the presence of water, where one can clearly see that the copper-exchanged sample is considerably more active than the Na-SSZ-13 and Fe-SSZ-13 samples.

Based on the results from the flow reactor experiments shown above, the choice of metal introduced into the SSZ-13 framework is decisive for the catalytic performance for NH_3-SCR. The utterly different catalytic behaviors of the Na-SSZ-13, Cu-SSZ-13 and Fe-SSZ-13 samples for NH_3-SCR can likely be explained mainly by the nature of the metal, hence, the active sites introduced into the zeolite framework. It is clearly seen that the active sites of copper promote NO_x reduction in a wide temperature range, even at low temperatures, while the active sites of iron promote the NO_x reduction only at high temperatures (above 400 °C). Sodium does not promote NO_x reduction at all.

When comparing the results of the flow reactor experiments with the results of the NH_3-TPD study, it can be seen that the type of exchange metal affects not only the reactions in the NH_3-SCR process but also the acidity of the zeolite. The acid sites have several roles, including enhancing both ammonia adsorption, which is needed for the NH_3-SCR reaction to take place, and NO oxidation to NO_2, which promotes the so-called fast SCR reaction.[3] Indeed, our results show that the NH_3-SCR activity generally increases with increased NH_3 adsorption capacity of the metal ion-exchanged SSZ-13 samples.

When considering the activity profiles for NH_3 oxidation and NO oxidation, they are found to be similar for all samples but with discrepancy in the highest conversion value that can be reached. This leads to the conclusion that the nature of the active metal sites is not of such crucial importance for the NH_3 and NO oxidation reactions as for the NH_3-SCR reaction where considerably different catalytic behaviors are observed for the samples containing different metals. In the absence of water, the Na-SSZ-13 sample is the least active for both NH_3 and NO oxidation, while Cu-SSZ-13 is the most active sample, although in the presence of water, the difference in activity for NO oxidation of the samples is not so strongly pronounced as in the absence of water.

Concluding remarks

In this work, the zeolite SSZ-13 in sodium form was synthesized under hydrothermal conditions based on the method previously reported by Zones.[16] However, by using a 25% lower amount of the structure-directing agent, *N*,*N*,*N*-trimethyl-1-adamantanammonium hydroxide, the yield of the zeolite product is just 9% lower than that in the reference method.[16] This shows one possible way to improve the synthesis of SSZ-13 in order to use less SDA and to achieve higher relative yield of the zeolite.

Subsequently, the synthesized Na-SSZ-13 material was ion-exchanged with iron and copper. After the ion exchange, the physicochemical properties of the prepared samples were characterized by different techniques including XRD, SEM, XRF, and UV-vis spectroscopy, BET, and NH_3-TPD. It was found that relatively large iron oxide particles are formed as a result of ion exchange with iron. However, for the Cu-SSZ-13 sample, the preparation procedure yielded highly dispersed ionic copper in the zeolite structure. The activity of the samples was then evaluated for selective catalytic reduction of NO_x with NH_3 as well as for NO oxidation and NH_3 oxidation, which are important side reactions of the NH_3-SCR process. The catalytic activity over the Cu- and Fe-exchanged SSZ-13 samples for NH_3-SCR was considerably higher compared to that over the parent Na-SSZ-13 sample. Hence, functionalization of the SSZ-13 structure with transition metal ions significantly enhances the catalytic activity. This is in agreement with previous studies and confirms the role of metal ions for the selective catalytic reduction over zeolites.

In particular, the Na-SSZ-13 (*i.e.* SSZ-13 in the form as it was synthesized) sample shows only negligible activity for NO_x reduction. However, the copper-exchanged sample, Cu-SSZ-13, shows very high activity for the NH_3-SCR reaction even at low temperatures. This is related to high NH_3-storage capacity and the small size of the copper oxide clusters on the copper-exchanged SSZ-13 sample. Concerning the iron-exchanged SSZ-13 sample, the activity is significantly higher at high temperatures than at low temperatures and the overall catalytic activity is lower than over the copper-exchanged SSZ-13 sample. This is related to the formation of a relatively high fraction of large iron oxide clusters, which previously have been shown to be inactive in NH_3-SCR. However, SSZ-13 may be functionalized by a combination of, *e.g.* copper and iron to widen the temperature window for NO_x reduction.

Acknowledgements

This work has been performed in the Competence Centre for Catalysis (KCK), which is located at the Chalmers University of Technology, and was financially supported by the Swedish Energy Agency and the member companies AB Volvo, ECAPS AB, Haldor Topsøe A/S, Scania CV AB and Volvo Car Corporation AB.

References

1 A. Cuperman, A. Kustov and L. Kustov, in *Zeolites and Zeolite-like Materials: Quo Vadis?*, ed. L. Kustov, Moscow State University, 2013, pp. 391–461.
2 J. Ochońska, D. McClymont, P. J. Jodłowski, A. Knapik, B. Gil, W. Makowski, W. Łasocha, A. Kołodziej, S. T. Kolaczkowski and J. Łojewska, *Catal. Today*, 2012, **191**, 6–11.
3 S. Brandenberger, O. Krocher, A. Tissler and R. Althoff, *Catal. Rev.: Sci. Eng.*, 2008, **50**, 492–531.
4 U. De La Torre, B. Pereda-Ayo and J. R. González-Velasco, *Chem. Eng. J.*, 2012, **207–208**, 10–17.
5 P. J. Andersen, J. E. Baille, J. L. Casel, H.-Y. Chen, J. M. Fedeyko, R. K. S. Foo and R. R. Rajaram, *Transition Metal/Zeolite SCR Catalysts*, Johnson Matthey Public Limited Company, USA, US 2010/0290963 A1, 2010.
6 T. Johnson, Diesel Emission Control in Review, *SAE [Tech. Pap.]*, 2001, 2001-01-0184, DOI: 10.4271/2001-01-0184.
7 M. Hesser, H. Lüders and R.-S. Henning, SCR Technology for NOx Reduction: Series Experience and State of Development, *DEER Conference*, 2005.
8 J. H. Kwak, R. G. Tonkyn, D. H. Kim, J. Szanyi and C. H. F. Peden, *J. Catal.*, 2010, **275**, 187–190.
9 D. W. Fickel, E. D'Addio, J. A. Lauterbach and R. F. Lobo, *Appl. Catal., B*, 2011, **102**, 441–448.
10 J. H. Li, H. Z. Chang, L. Ma, J. M. Hao and R. T. Yang, *Catal. Today*, 2011, **175**, 147–156.
11 J. H. Kwak, J. H. Lee, D. Tran, R. R. Tonkyn, J. Szanyi and C. H. F. Peden, *Abstr. Pap. Am. Chem. Soc.*, 2011, **242**.
12 D. W. Fickel, E. D'Addio, J. A. Lauterbach and R. F. Lobo, *Appl. Catal., B*, 2011, **102**, 441–448.
13 A. V. Kucherov and A. A. Slinkin, *J. Mol. Catal.*, 1994, **90**, 323–354.
14 I. Melián-Cabrera, S. Espinosa, J. C. Groen, B. v/d Linden, F. Kapteijn and J. A. Moulijn, *J. Catal.*, 2006, **238**, 250–259.
15 S. I. Zones, *Zeolite SSZ-13 and its method of preparation*, USA, US4544538 A, 1985.
16 International Zeolite Association web-page, http://www.iza-online.org (last time accessed: 2013, December, 8).
17 L. Wu, V. Degirmenci, P. C. M. M. Magusin, N. J. H. G. M. Lousberg and E. J. M. Hensen, *J. Catal.*, 2013, **298**, 27–40.
18 F. Gao, E. D. Walter, E. M. Karp, J. Luo, R. G. Tonkyn, J. H. Kwak, J. Szanyi and C. H. F. Peden, *J. Catal.*, 2013, **300**, 20–29.
19 Z. Liu, Y. Wang and Z. Xie, *Cuihua Xuebao*, 2012, **33**, 22–38.
20 Y. Marcus, *J. Solution Chem.*, 1983, **12**, 271–275.
21 C. Suryanarayana and M. G. Norton, *X-Ray Diffraction: A Practical Approach*, Plenum Press, New York, 1998, pp. 52–60.
22 G. Delahay, D. Valade, A. Guzman-Vargas and B. Coq, *Appl. Catal., B*, 2005, **55**, 149–155.
23 L. Sommer, D. Mores, S. Svelle, M. Stöcker, B. M. Weckhuysen and U. Olsbye, *Microporous Mesoporous Mater.*, 2010, **132**, 384–394.
24 R. K. Iler, *The Chemistry Of Silica: Solubility, Polymerization, Colloid and Surface Properties, and Biochemistry*, Wiley-Interscience, 1979, pp. 665–676.
25 S. Shwan, J. Jansson, L. Olsson and M. Skoglundh, *Appl. Catal., B*, 2014, **147**, 111–123.
26 R. Nedyalkova, S. Shwan, M. Skoglundh and L. Olsson, *Appl. Catal., B*, 2013, **138–139**, 373–380.
27 M. S. Kumar, M. Schwidder, W. Grünert and A. Brückner, *J. Catal.*, 2004, **227**, 384–397.
28 S. Brandenberger, O. Kröcher, A. Tissler and R. Althoff, *Appl. Catal., A*, 2010, **373**, 168–175.
29 S. Brandenberger, O. Kröcher, A. Tissler and R. Althoff, *Appl. Catal., B*, 2010, **95**, 348–357.
30 X. Zhou, H. Chen, X. Cui, Z. Hua, Y. Chen, Y. Zhu, Y. Song, Y. Gong and J. Shi, *Appl. Catal., A*, 2013, **451**, 112–119.
31 N. Liu, R. Zhang, B. Chen, Y. Li and Y. Li, *J. Catal.*, 2012, **294**, 99–112.
32 L. Martins, R. P. S. Peguin, M. Wallau and E. A. Urquieta-González, *J. Braz. Chem. Soc.*, 2005, **16**(3b), 589–596.
33 S. Bennici, A. Gervasini, N. Ravasio and F. Zaccheria, *J. Phys. Chem. B*, 2003, **107**, 5168–5176.
34 S. Kieger, G. Delahay, B. Coq and B. Neveu, *J. Catal.*, 1999, **183**, 267–280.
35 R. A. Schoonheydt, *Catal. Rev.: Sci. Eng.*, 1993, **35**, 129–168.
36 F. Gao, J. Kwak, J. Szanyi and C. F. Peden, *Top. Catal.*, 2013, **56**, 1441–1459.
37 M. E. Davis, *Ind. Eng. Chem. Res.*, 1991, **30**, 1675–1683.
38 T. Maesen, in *Studies in Surface Science and Catalysis*, ed. J. Čejka, H. V. Bekkum, A. Corma and F. Schüth, Elsevier, 2007, pp. 1–12.
39 J. Rouquerol, P. Llewellyn and F. Rouquerol, in *Studies in Surface Science and Catalysis*, ed. P. L. Llewellyn, F. Rodriquez-Reinoso, J. Rouqerol and N. Seaton, Elsevier, 2007, pp. 49–56.
40 M. Thommes, in *Studies in Surface Science and Catalysis*, ed. J. Čejka, H. V. Bekkum, A. Corma and F. Schüth, Elsevier, 2007, vol. 168, pp. 495–523.
41 H.-Y. Jeon, C.-H. Shin, H. J. Jung and S. B. Hong, *Appl. Catal., A*, 2006, **305**, 70–78.
42 A. Zecchina, S. Bordiga, J. G. Vitillo, G. Ricchiardi, C. Lamberti, G. Spoto, M. Bjørgen and K. P. Lillerud, *J. Am. Chem. Soc.*, 2005, **127**, 6361–6366.
43 O. A. Anunziata, A. R. Beltramone, Z. Juric, L. B. Pierella and F. G. Requejo, *Appl. Catal., A*, 2004, **264**, 93–101.
44 A. Shishkin, P.-A. Carlsson, H. Härelind and M. Skoglundh, *Top. Catal.*, 2013, **56**, 567–575.
45 B. Pereda-Ayo, U. De La Torre, M. J. Illán-Gómez, A. Bueno-López and J. R. González-Velasco, *Appl. Catal., B*, 2014, **147**, 420–428.

46 S. Shwan, R. Nedyalkova, J. Jansson, J. Korsgren, L. Olsson and M. Skoglundh, *Top. Catal.*, 2013, **56**, 80–88.
47 A. Sultana, T. Nanba, M. Haneda, M. Sasaki and H. Hamada, *Appl. Catal., B*, 2010, **101**, 61–67.
48 P. S. Metkar, M. P. Harold and V. Balakotaiah, *Chem. Eng. Sci.*, 2013, **87**, 51–66.
49 T. Komatsu, M. Nunokawa, I. S. Moon, T. Takahara, S. Namba and T. Yashima, *J. Catal.*, 1994, **148**, 427–437.
50 R. Nedyalkova, K. Kamasamudram, N. W. Currier, J. Li, A. Yezerets and L. Olsson, *J. Catal.*, 2013, **299**, 101–108.
51 M. Ruggeri, I. Nova and E. Tronconi, *Top. Catal.*, 2013, **56**, 109–113.
52 M. Colombo, I. Nova, E. Tronconi, V. Schmeißer, B. Bandl-Konrad and L. Zimmermann, *Appl. Catal., B*, 2012, **111–112**, 106–118.
53 P. S. Metkar, V. Balakotaiah and M. P. Harold, *Chem. Eng. Sci.*, 2011, **66**, 5192–5203.